Frontiers in Bioscience Landmark

Front. Biosci. (Landmark Ed) **2026**; 31(9): 52485
https://doi.org/10.31083/FBL52485

Original Research

Multi-Omics Analysis and Experimental Validation Uncover Neddylation-Associated Biomarkers and Cellular Landscape in Lung Adenocarcinoma

Xiaogang Peng[1,2], Guangming Xiang[2], Gengyun Sun[1,*]

[1]Department of Respiratory and Critical Care Medicine, The First Affiliated Hospital of Anhui Medical University, 230022 Hefei, Anhui, China
[2]Department of Respiratory and Critical Care Medicine, Yichang Central People's Hospital, 443000 Yichang, Hubei, China
*Correspondence: sungengyun@ahmu.edu.cn (Gengyun Sun)

Academic Editors: Erika Di Zazzo and Sung Eun Kim
Submitted: 1 April 2026 Revised: 25 June 2026 Accepted: 7 July 2026 Published: 17 September 2026

Abstract

Background: Accumulating evidence suggests that neddylation contributes to tumor initiation and progression. Nonetheless, its biological functions and regulatory mechanisms in lung adenocarcinoma (LUAD) remain poorly understood. **Methods:** Bioinformatics analyses integrated single-cell RNA sequencing (scRNA-seq) datasets from the Gene Expression Omnibus (GEO) with bulk RNA-seq data from The Cancer Genome Atlas (TCGA). The Seurat package was used for scRNA-seq processing, including cell clustering, annotation, cell-cell interaction analysis, and pseudotime trajectory inference. The survival and pROC packages were used for Kaplan–Meier (KM) survival and receiver operating characteristic (ROC) analyses, respectively. Tissue microarray (TMA) and immunohistochemistry (IHC) analyses were performed to validate biomarker expression. Functional assays, including Cell Counting Kit-8 (CCK-8), colony formation, wound healing, and Transwell assays, were conducted in A549 and NCI-H1975 cells with DNAJB1 knockdown. **Results:** Eight major cell populations were identified at the single-cell level, among which T/NK cells, particularly CD8+ effector memory T cells (CD8+ Tem), exhibited strong associations with neddylation. T/NK cells displayed extensive ligand-receptor-mediated interactions with other cell types. A transcription factor (TF)–target regulatory network was constructed, revealing that Surfactant Protein C (SFTPC), Lipopolysaccharide-Induced TNF Factor (LITAF), Serine/Threonine Kinase 17B (STK17B), Enah/Vasp-Like Protein (EVL), FYN Proto-Oncogene, Src Family Tyrosine Kinase (FYN), and Lymphocyte-Specific Protein 1 (LSP1) were associated with favorable prognosis, whereas DNAJB1 correlated with poor survival in LUAD patients. Pseudotime trajectories further delineated dynamic differentiation pathways of T/NK subsets and differential TF target expression across states. IHC analysis showed elevated DNAJB1 expression in tumors compared with adjacent normal tissues. Moreover, silencing DNAJB1 significantly inhibited proliferation, migration, and invasion in A549 and NCI-H1975 cells. **Conclusion:** This study identifies neddylation-associated cellular phenotypes and clinically relevant biomarkers in LUAD, providing new mechanistic insights and highlighting potential therapeutic targets for LUAD treatment.

Keywords: neddylation; lung adenocarcinoma; single-cell RNA sequencing; DNAJB1; tumor microenvironment; T/NK cells

1. Introduction

Lung cancer continued to be the leading cancer diagnosis in 2022, with close to 2.5 million new cases, making up roughly one-eighth of all cancer diagnoses worldwide [1]. The distribution included 717,211 adenocarcinoma cases (45.6%), 461,171 squamous cell carcinoma (SCC) cases (29.4%), 180,063 small-cell carcinoma cases (11.5%), and 101,861 large-cell carcinoma cases (6.5%), indicating that lung adenocarcinoma (LUAD) continues to represent the predominant histological subtype [2]. In most countries, less than 20% of people with lung cancer survive for five years [3]. Known risk factors are secondhand smoke, exposure to radon, air pollution, asbestos, and having a family history of lung cancer in immediate family members [4]. Treatment options mainly consist of surgery, radiotherapy, and systemic therapies, which are often combined based on disease stage and require multidisciplinary decision-making [5,6]. CT-guided core-needle biopsy (CNB) is widely used for pathological diagnosis of pulmonary lesions, showing high diagnostic accuracy and acceptable safety across diverse lesion types, including complex lesions such as those associated with cystic airspaces [7,8]. Therefore, identifying more reliable biomarkers and elucidating the underlying molecular mechanisms are urgently needed to improve the effectiveness of current therapeutic strategies for LUAD [9,10].

Neddylation is a type of post-translational modification where the ubiquitin-like protein NEDD8 attaches to substrate proteins, influencing various crucial biological functions [11,12]. Like ubiquitination, the neddylation process involves three enzymatic stages: the ATP-dependent creation of an E1-NEDD8 thioester intermediate, the transfer of NEDD8 from E1 to the catalytic cysteine of E2 through transthioesterification, and the following interaction of the E2-NEDD8 complex with an E3 ligase that aids in attaching NEDD8 to target proteins [13,14]. Accumulating evidence highlights the critical roles of neddylation in tumorigenesis, progression, and metastasis [15]. The ned-

Copyright: © 2026 The Author(s). Published by IMR Press.
This is an open access article under the CC BY 4.0 license.

Publisher's Note: IMR Press stays neutral with regard to jurisdictional claims in published maps and institutional affiliations.

dylation pathway promotes tumor progression by regulating multiple cellular responses, including tumor cell proliferation and metabolism [16], and by modulating immune functions within the tumor microenvironment (TME), such as T cell activation, proliferation, differentiation, and survival [17]. These findings support the notion that inhibition of the neddylation pathway represents a novel and promising anti-tumor therapeutic strategy [18].

The process of neddylation modifies proteins after translation to influence their function and stability [12]. Aberrant activation or overexpression of components within the neddylation pathway can lead to the stabilization of oncoproteins and the destabilization of tumor suppressor proteins, thereby altering multiple signaling pathways that collectively drive cancer development and progression [18,19]. In recent years, the neddylation pathway has emerged as a druggable target for therapeutic intervention. Several compounds that inhibit neddylation have been identified, including inhibitors of NEDD8-activating enzyme (NAE). Pevonedistat, also referred to as MLN4924, is presently in Phase I/II/III clinical trials aimed at treating different types of human cancers [15,20]. Therefore, targeting the neddylation pathway offers a promising strategy to selectively influence protein degradation and represents an attractive option for developing anticancer drugs. However, several key questions remain unresolved in LUAD, including the prognostic relevance of neddylation-related gene signatures, their impact on tumor microenvironment composition, and the functional and mechanistic role of Neddylation-related biomarkers in LUAD progression.

This research involved an in-depth examination of single-cell RNA sequencing (scRNA-seq) and bulk RNA-seq data to pinpoint neddylation-associated cell populations and biomarkers in the TME of LUAD. In addition, tissue microarray (TMA) and immunohistochemistry (IHC) staining were conducted to validate biomarker expression. Finally, *in vitro* experiments were performed to investigate the functional roles of these biomarkers.

2. Materials and Methods

2.1 Data Gathering

Single-cell RNA-sequencing (scRNA-seq) data for LUAD patients, which is publicly accessible, were obtained from the Gene Expression Omnibus (GEO). From the GSE131907 dataset, 11 primary lung tumor tissues and 11 normal lung tissues were included in this study. Specifically, the tumor samples correspond to GSM3827125, GSM3827126, GSM3827127, GSM3827128, GSM3827129, GSM3827130, GSM3827131, GSM3827132, GSM3827133, GSM3827134, GSM3827135, and the normal lung tissues correspond to GSM3827114, GSM3827115, GSM3827116, GSM3827117, GSM3827118, GSM3827119, GSM3827120, GSM3827121, GSM3827122, GSM3827123, GSM3827124.

Additionally, data on gene expression from 450 LUAD tumor samples and 59 nearby normal samples were obtained from the Cancer Genome Atlas (TCGA, https://www.cancer.gov/about-nci/organization/ccg/research/structural-genomics/tcga). Sequencing data (read count) and clinical details for LUAD patients were sourced from the UCSC Xena website (https://xenabrowser.net/datapages/).

Moreover, a total of 260 Neddylation related genes (NeddGs) were retrieved from the Molecular Signatures Database (MSigDB, https://www.gsea-msigdb.org/gsea/msigdb/) (**Supplementary Table 1**).

2.2 Processing and Annotating Data From Single-Cell RNA Sequencing (scRNA-seq)

All scRNA-seq data in this study were processed and analyzed using the "Seurat" package (v5.2.1) in R. The "CreateSeuratObject ()" function was used to generate the initial object and filter cells. Cells with under 200 genes expressed and genes present in fewer than ten cells were eliminated from the dataset. Cells with over 20% mitochondrial gene content were discarded, and cells expressing 100 to 8000 genes were retained using the "PercentageFeatureSet" function. After these quality control steps, an expression matrix containing 88,144 cells and 22,973 genes was obtained for downstream analyses.

Data were normalized with the "NormalizeData" function, while highly variable genes were detected using the "FindVariableFeatures" function. Batch correction was conducted with the "Harmony" package (v1.2.3). Before performing principal component analysis (PCA), the "ScaleData" function was applied for data scaling, and the top 30 principal components were then used for uniform manifold approximation and projection (UMAP). Using a resolution range of 0.1 to 1.5, unsupervised clustering was performed with the "FindNeighbors" and "FindClusters" functions, and dimensionality reduction was carried out using "RunUMAP". Cell type annotation employed the "FindAllMarkers" function, relying on canonical marker genes from the CellMarker database (http://117.50.127.228/CellMarker/).

2.3 Calculation of the Neddylation Score (Nedd-Score)

The differentially expressed NeddGs for each cell between LUAD tumor lung tissues and normal lung tissues were calculated using the Wilcoxon test with false discovery rate (FDR) <0.05 and |log2 fold change (FC)| >0. Then, the "AddModuleScore" function was used to calculate the Nedd-score for each cell according to these differentially expressed NeddGs. Furthermore, cell type with the highest Nedd-score was selected for cell reannotation using "RunAUCell" function.

2.4 Functional Enrichment Analysis for Sub-Cell Types

The Gene Set Variation Analysis (GSVA) algorithm was used to assess pathway activity across different cell types. Gene sets from the Kyoto Encyclopedia of Genes and Genomes (KEGG) (c5.all.v7.4.symbols.gmt) were obtained from the Molecular Signatures Database (MSigDB) for functional enrichment analysis. In addition, cytokine signaling pathway activity was evaluated using the Cytokine Signaling Analyzer (CytoSig) [21]. The "ssGSEA" function in the GSVA package (v2.0.5) was applied to calculate enrichment scores for each pathway at the single-cell level. Pathways with a p-value < 0.05 were considered significantly enriched.

2.5 Communication From One Cell to Another

The "CellChat" package version 1.6.1 was employed to explore possible interactions between various cell types. Based on a curated human ligand-receptor database and pattern recognition methods, "CellChat" forecasts key signaling inputs and outputs, revealing how cell groups manage their functional states. Pairs of ligands and receptors with a p-value less than 0.05 were kept to evaluate communication links between cell types.

2.6 Construction of a Gene Regulatory Network

Transcription factor (TF) activity was inferred using a combination of "DoRothEA" (v. 1.18.0) and "VIPER" (v. 1.40.0) [22]. The top 20 TFs in cell types with the highest Nedd-scores were selected to construct a TF-target regulatory network using Cytoscape (v3.10.0).

2.7 Pseudotime Trajectory Analysis

The "Monocle" (v. 2.36.0) package was used to perform pseudotime trajectory analysis to characterize functional changes in cell types with the highest Nedd-scores and to determine potential lineage differentiation. In addition, Branched Expression Analysis Modeling (BEAM) was conducted to identify genes that vary at differentiation branch points [23]. Branching-related genes were visualized using the heatmap package (v1.0.12) in R, which generated heatmaps of differentially expressed branching genes [24].

2.8 Prognosis Analysis of Nedd-Score-Related Transcription Factors Based on Bulk RNA-seq Data

The "survival" package (v3.6-4) facilitated Kaplan-Meier (KM) survival analysis to explore associations between transcription factors (TFs) and overall survival (OS). The "pROC" package (v1.19.0.1) was used to conduct a receiver operating characteristic (ROC) curve analysis to evaluate the predictive sensitivity and specificity of cell clusters in the training cohort.

2.9 Tissue Microarray (TMA) and Immunohistochemistry (IHC)

The expression of DNAJB1 was evaluated using a tissue microarray (TMA; HlugA150CS04) comprising 150 samples, including 75 tumor tissues and 75 matched adjacent non-tumor tissues, along with corresponding clinical data. The TMA was obtained from Shanghai OUTDO Biotech Co., Ltd. (Lot No. XT23-003, Shanghai, China). All tissue samples were collected with informed consent at enrollment.

The patients ranged in age from 35 to 77 years and included 42 males and 33 females. Histopathological analysis revealed that all cases were adenocarcinomas, among which 9 cases were accompanied by bronchioloalveolar carcinoma, 1 case was papillary adenocarcinoma, and 1 case was mucinous adenocarcinoma. In addition, clinicopathological parameters, including tumor size, depth of invasion, lymphatic invasion, vascular invasion, pathological grade, and clinical stage, were also collected and analyzed. The detailed information on the clinical characteristics of the patient samples is shown in Table 1.

Table 1. Clinicopathological characteristics of paired tumor microarray (TMA) cohort (n = 75 patients).

Variable	Category	n (%)/Mean ± SD
Age (years)		58.3 ± 11.2
Gender	Male	42 (56.0%)
	Female	33 (44.0%)
Tissue type	Paired samples	75 (100%)
Tumor site	Right lung	40 (53.3%)
	Left lung	32 (42.7%)
	Central/bilateral	3 (4.0%)
Tumor size (cm)		4.1 ± 2.2
Histological type	Adenocarcinoma	75 (100%)
Pathological grade	I–II	15 (20.0%)
	II	24 (32.0%)
	II–III	29 (38.7%)
	III	7 (9.3%)
T stage	T1–T2	52 (69.3%)
	T3–T4	23 (30.7%)
N stage	N0	60 (80.0%)
	N1–N3	15 (20.0%)
M stage	M0	70 (93.3%)
	M1	5 (6.7%)
AJCC stage (7th)	I	30 (40.0%)
	II	22 (29.3%)
	III	18 (24.0%)
	IV	5 (6.7%)

AJCC stage, American Joint Committee on Cancer stage.

Immunohistochemical (IHC) staining was performed using a primary anti-DNAJB1 antibody (1:500 dilution).

DNAJB1 expression was semi-quantitatively evaluated using the histochemistry score (H-score), calculated as ∑(pi × i), where i represents staining intensity (0 = negative, 1 = weak, 2 = moderate, 3 = strong), and pi indicates the percentage of cells at each intensity level. The H-score was defined as: (percentage of weak-intensity cells × 1) + (percentage of moderate-intensity cells × 2) + (percentage of strong-intensity cells × 3). Higher H-scores indicate stronger overall staining intensity.

2.10 Cell Line, Cell Culture, and Transfection

Cell lines A549 and NCI-H1975 were purchased from Procell (Wuhan, China). All cell lines used in this study were authenticated by STR profiling and routinely tested negative for mycoplasma contamination. Cells were cultured in complete RPMI-1640 medium (Servicebio, Wuhan, China) supplemented with 10% fetal bovine serum (FBS; Gibco, MA, USA) and 1% penicillin-streptomycin solution (Gibco, MA, USA). All cells were maintained in a humidified incubator at 37 °C with 5% CO_2.

Human DNAJB1 shRNA constructs (sh-DNAJB1 #1: 5′-CGGCTGTACCAAGAAGATGAA-3′; sh-DNAJB1 #2: 5′-CGTCGTATTCAAAGATGTTAT-3′; sh-DNAJB1 #3: 5′-CGACGGAAAGAGCATTCGAAA-3′) and the corresponding control shRNA lentiviral plasmid were obtained from Shanghai GeneChem Co., Ltd. (Shanghai, China). Cell transfections were performed using Lipofectamine 2000 (Invitrogen, CA, USA) according to the manufacturer's instructions.

2.11 RNA Extraction and qPCR

Total RNA was extracted from cells using Trizol reagent (Life Technologies Corporation, MD, USA) following the manufacturer's instructions. Complementary DNA (cDNA) was synthesized using the TaqMan MicroRNA Reverse Transcription Kit (Applied Biosystems, CA, USA) according to the standard protocol. Quantitative PCR (qPCR) was then performed using Taq Pro Universal SYBR qPCR Master Mix (Vazyme, Nanjing, China) following the manufacturer's instructions. PCR amplification was carried out on a QuantStudio™ 5 Real-Time PCR Instrument (Applied Biosystems, MA, USA) using the following program: 95 °C for 15 s, followed by 40 cycles of 95 °C for 15 s and 60 °C for 30 s. GAPDH was used as the internal reference. Relative gene expression levels were calculated using the $2^{-\Delta\Delta Ct}$ method. The primer sequences used in this study were as follows: DNAJB1: forward 5′-GACCTCCAACAACATTCC-3′, reverse 5′-ATGACATCAGAGCCATCT-3′; GAPDH: forward 5′-TTGCCCTCAACGACCACTTT-3′, reverse 5′-TGGTCCAGGGGTCTTACTCC-3′.

2.12 Cell Viability Analysis

The Cell Counting Kit-8 (CCK-8) assay was used to evaluate cell viability. In short, cells were plated in 96-well plates at a concentration of 500 cells per well and transfected with shRNA lentiviral plasmids for 0, 24, 48, and 72 h. A CCK-8 solution from Beyotime in Shanghai, China, was added to each well and incubated at 37 °C for two hours. Afterward, the absorbance at 450 nm was measured with a microplate reader.

2.13 Cell Colony Formation

After transfection for 24 h, tumor cells were seeded into 6-well plates at a density of 500 cells per well to assess colony formation ability. Cells were cultured for 2 weeks, then fixed with methanol and stained with 0.1% crystal violet. The number of colonies was subsequently counted.

2.14 Cell Migration and Invasion

In vitro cell migration and invasion were evaluated using wound healing and Transwell assays, as previously described with minor modifications. For wound healing assays, after transfection 24 h, cells were seeded into 6-cm culture dishes and grown to a near-confluent monolayer. A 10-µL pipette tip was used to create a scratch across the center of each dish, and cellular debris was removed by washing with phosphate-buffered saline (PBS). Cultures were then incubated at 37 °C and photographed at 0 and 48 h. The percentage of wound closure relative to 0 h was quantified using Image J 1.54 (National Institutes of Health, Bethesda, MD, USA).

For Transwell assay, after transfection 24 h, cells were serum-starved, detached, and resuspended in serum-free medium. A 100-µL cell suspension was added to the upper chamber of a Transwell insert (8.0 µm pore size; Corning, NY, USA), and medium containing 20% FBS was added to the lower chamber. After 36 h, non-migrated cells on the upper surface of the membrane were removed, and cells on the undersurface were fixed and stained with 5% crystal violet. Images were captured from each membrane, and invasive cells were counted under a microscope.

2.15 Statistical Analysis

All data processing and statistical analyses were conducted using R software (version 4.3.1; R Foundation for Statistical Computing; https://www.r-project.org/). Statistical analyses were performed using GraphPad Prism software (version 9.0, San Diego, CA, USA). Data are presented as mean ± standard deviation (SD). Comparisons between two groups were conducted using Student's *t*-test, while comparisons among multiple groups were performed using one-way or two-way analysis of variance (ANOVA) as appropriate. A p-value < 0.05 was considered statistically significant.

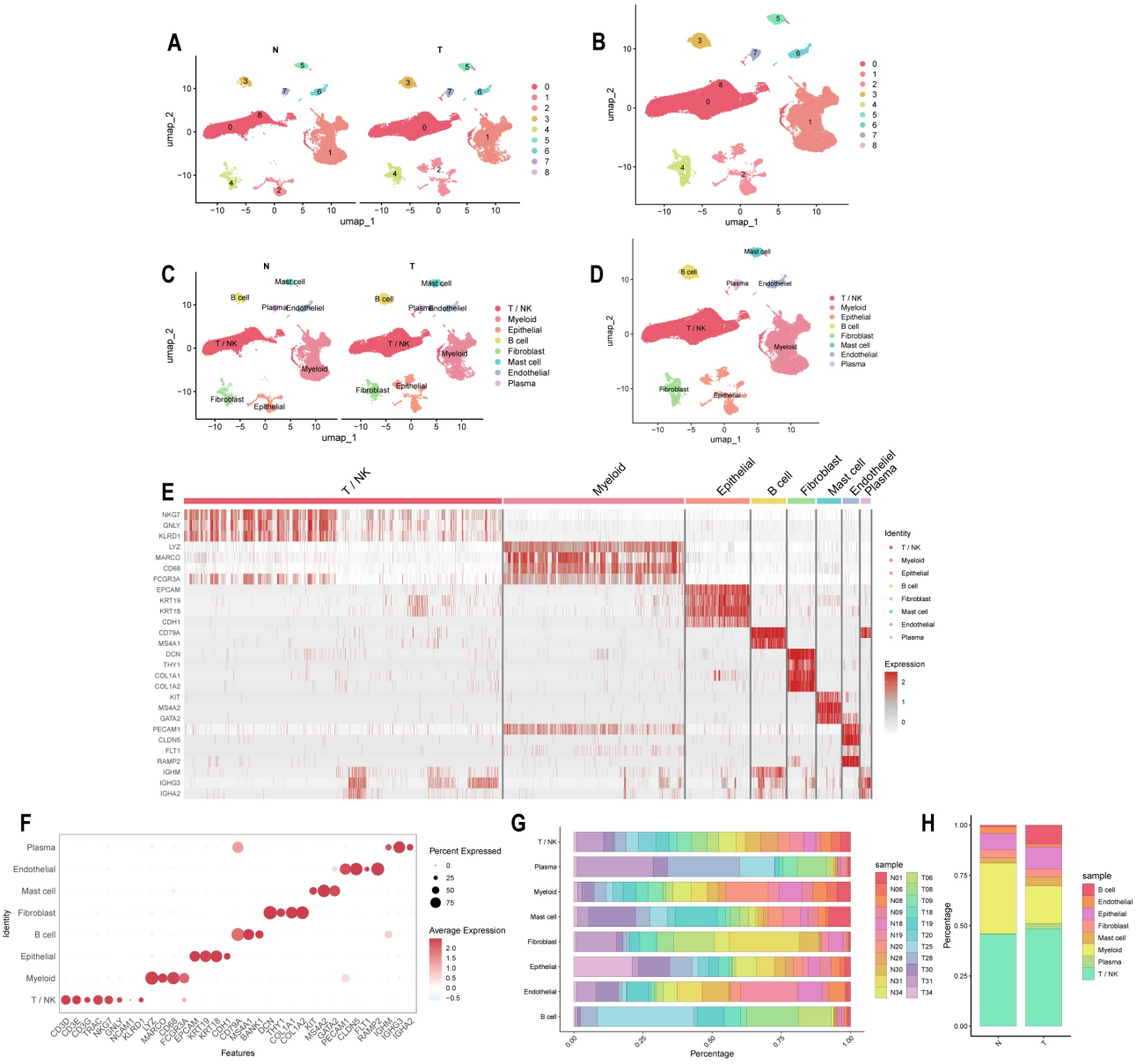

Fig. 1. Identification of eight major cell populations in lung adenocarcinoma (LUAD). (A) Uniform manifold approximation and projection (UMAP) visualization of nine unsupervised cell clusters in tumor and normal samples, shown separately. (B) UMAP visualization of nine cell clusters across all samples. (C) UMAP visualization of eight major cell populations in tumor and normal samples, shown separately. (D) UMAP visualization of eight major cell populations across all samples. (E) Heatmap showing the average expression levels and percentage of marker gene expression across each annotated cell type. (F) Bubble plot illustrating the average expression levels and proportion of marker gene expression in each cell type. (G) Proportional distribution of each cell type in tumor versus normal tissues across individual samples. (H) Overall comparison of cell type proportions between tumor and normal tissues.

3. Results

3.1 Identification of Eight Major Cell Populations in Lung Adenocarcinoma (LUAD)

To delineate the cellular ecosystem of the LUAD tumor microenvironment (TME) at single-cell resolution, we analyzed the scRNA-seq dataset GSE131907. After quality control, normalization, dimensionality reduction, and unsupervised clustering (**Supplementary Fig. 1A–E**), a total of 88,144 high-quality cells were retained and grouped into nine distinct clusters (Fig. 1A,B). The consistent distribution of clusters across samples suggested minimal batch effects, supporting the robustness of the dataset for downstream analyses.

Based on canonical lineage-specific marker genes (Fig. 1E,F), eight major cell populations were identified (Fig. 1C,D), including T/NK cells (CD3D, CD3E, TRAC,

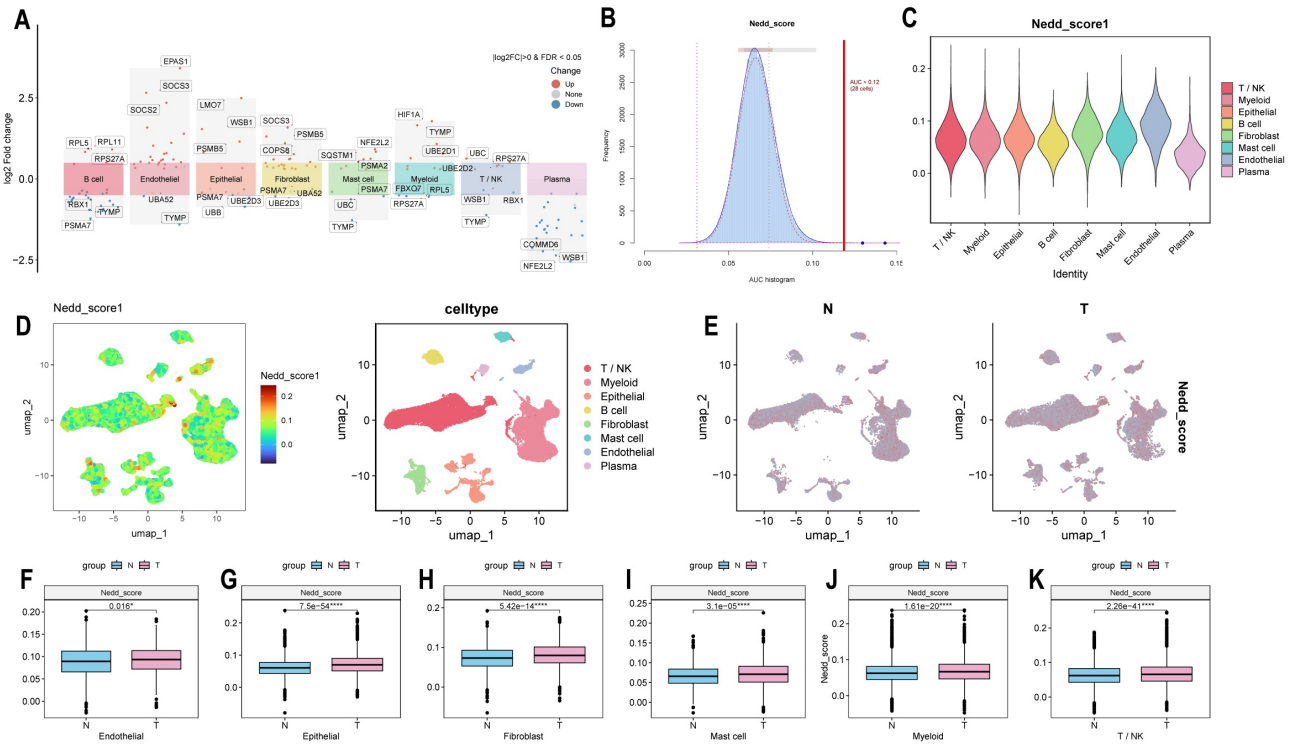

Fig. 2. Identification of T and NK cells as the predominant neddylation-associated cell populations in LUAD. (A) Differential expression analysis of neddylation-related genes (NeddGs), showing significantly up- and down-regulated genes across major cell types (FDR <0.05). (B) Computation of the neddylation score (Nedd-score) for each cell based on differentially expressed NeddGs. (C) Violin plot illustrating the distribution of Nedd-scores across different cell types. (D) UMAP visualization of Nedd-scores across all cell populations in all samples. (E) UMAP visualization of Nedd-scores stratified by tumor and normal tissues. (F) Comparison of Nedd-scores between tumor and normal tissues in endothelial cells. (G) Comparison of Nedd-scores between tumor and normal tissues in epithelial cells. (H) Comparison of Nedd-scores between tumor and normal tissues in fibroblasts. (I) Comparison of Nedd-scores between tumor and normal tissues in mast cells. (J) Comparison of Nedd-scores between tumor and normal tissues in myeloid cells. (K) Comparison of Nedd-scores between tumor and normal tissues in T/NK cells. Data are presented as mean ± SD. *$p < 0.05$ and ****$p < 0.0001$.

NKG7), myeloid cells (LYZ, MARCO, CD68, FCGR3A), epithelial cells (EPCAM, KRT19, KRT18, CDH1), B cells (CD79A, MS4A1, BANK1), fibroblasts (DCN, THY1, COL1A1, COL1A2), mast cells (KIT, MS4A2, GATA2), endothelial cells (PECAM1, CLDN5, FLT1, RAMP2), and plasma cells (IGHM, IGHG3, IGHA2). This cellular landscape reflects the complex multicellular architecture of the LUAD tumor microenvironment, comprising both immune and stromal compartments.

We next quantified cell-type composition differences between tumor and normal tissues. Compared with normal tissues, tumor samples exhibited increased proportions of B cells, epithelial cells, mast cells, plasma cells, and T/NK cells, whereas endothelial cells and myeloid cells were reduced (Fig. 1G,H). These shifts indicate a profound remodeling of the tumor microenvironment during LUAD progression, characterized by enhanced immune infiltration alongside depletion of certain myeloid and vascular-associated populations.

Collectively, these findings reveal a highly heterogeneous and dynamically reprogrammed tumor microenvironment in LUAD, providing a cellular foundation for subsequent analyses of neddylation-associated transcriptional and functional alterations.

3.2 Identification of T and NK Cells as the Predominant Neddylation-Associated Cell Populations in LUAD

To investigate the role of neddylation in LUAD, we first identified 57 differentially expressed neddylation-related genes (NeddGs) across major cell lineages between tumor and normal samples (Fig. 2A; **Supplementary Table 2**). A neddylation-related score (Nedd-score) was then calculated for each individual cell (Fig. 2B,C), and cells were stratified into high- and low-Nedd-score groups (Fig. 2D). We observed that T/NK cells, mast cells, endothelial cells, and fibroblasts were more enriched in the high-Nedd-score group compared with the low-Nedd-score group (Fig. 2D,E). Consistently, these cell populations exhibited significantly elevated Nedd-scores in tumor samples relative to

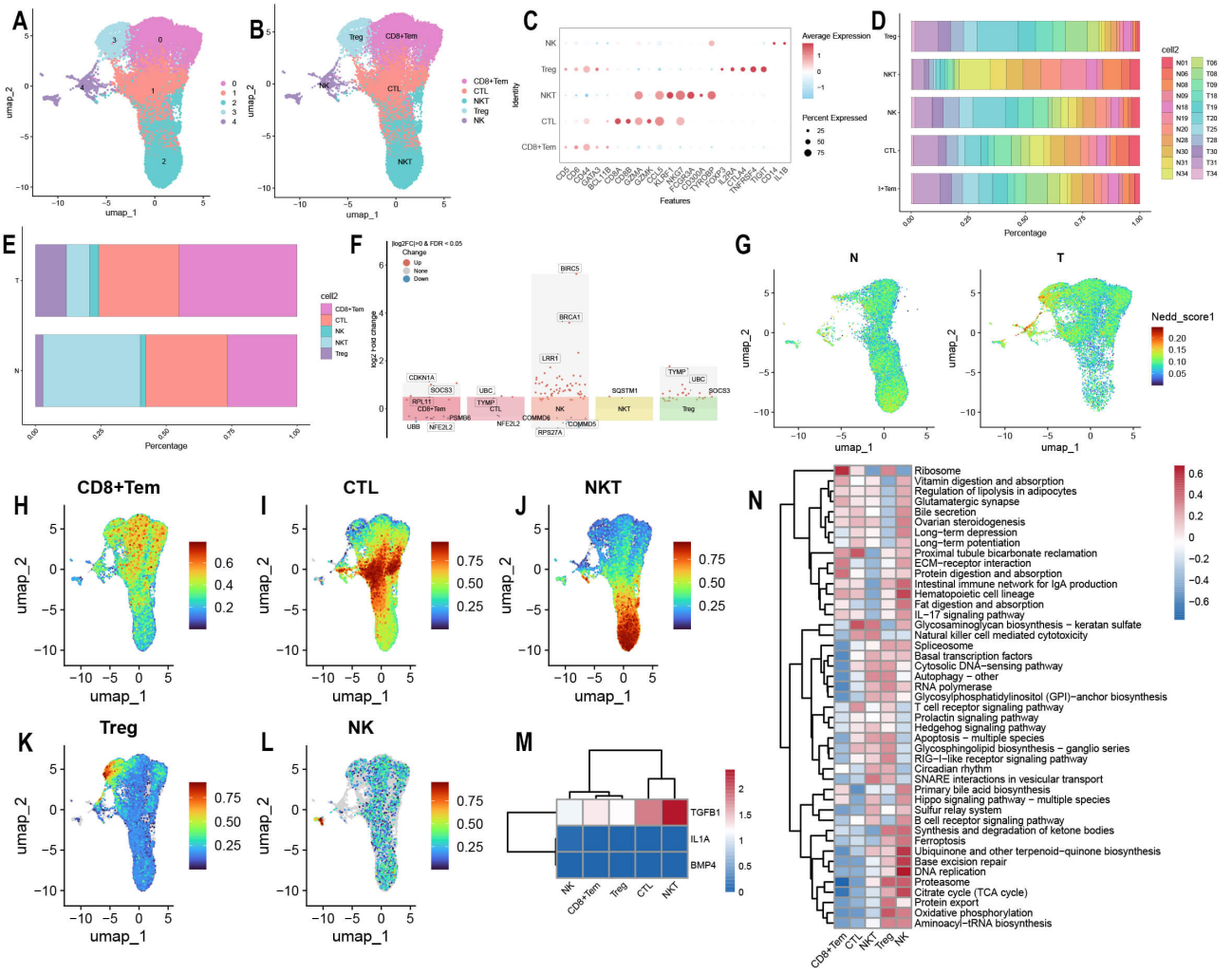

Fig. 3. Characteristics of T/NK subpopulations in LUAD. (A) UMAP visualization of five T/NK cell subclusters. (B) UMAP visualization of five annotated T/NK cell subtypes. (C) Bubble plot showing the average expression levels and proportion of marker genes across T/NK cell subtypes. (D,E) Proportional distribution of T/NK cell subtypes in tumor versus normal tissues. (F) Differential expression analysis of neddylation-related genes (NeddGs) across T/NK cell subtypes (FDR <0.05). (G) UMAP visualization of Nedd-scores across T/NK cell subtypes in tumor and normal samples. (H–L) UMAP visualization of Nedd-scores in (H) effector memory CD8+ T cells (CD8+ Tem), (I) cytotoxic T cells (CTL), (J) natural killer T cells (NKT), (K) regulatory T cells (Treg), and (L) natural killer (NK) cells. (M) Heatmap depicting CytoSig-based cytokine signaling activity across T/NK cell subtypes. (N) Heatmap showing KEGG pathway enrichment profiles across T/NK cell subtypes.

normal samples (Fig. 2F–K). Taken together, these findings indicate that T/NK cells represent the predominant immune cell population associated with elevated neddylation activity, highlighting a potential role of neddylation in shaping the immune landscape of LUAD.

3.3 Characteristics of T/NK Subpopulations in LUAD

To further dissect the heterogeneity of neddylation activity within T/NK cells, we identified five distinct subclusters, including effector memory CD8+ T cells (CD8+ Tem; CD6, CD44), cytotoxic T cells (CTL; CD8A, GZMA, CCL5), regulatory T cells (Treg; TNFRSF4, TIGIT), natural killer (NK) cells (NKG7, KLRD1, FCGR3A, TYROBP), and natural killer T (NKT) cells (CCL5, NKG7, KLRD1, FCGR3A) (Fig. 3A–C).

Comparative analysis between tumor and normal tissues revealed a reshaping of the T/NK compartment, characterized by expansion of CD8+ Tem, Treg, and NK cells, and reduction of NKT cells in tumors (Fig. 3D,E), suggesting an imbalance between effector and regulatory immune states in the LUAD microenvironment.

We next evaluated neddylation-associated transcriptional activity across subclusters and identified 73 differentially expressed NeddGs (Fig. 3F; **Supplementary Table 3**). Single-cell Nedd-score analysis further revealed that CD8+ Tem cells exhibited the highest neddylation activity

among all T/NK subsets (Fig. 3G–L), indicating that this subset may represent a key effector population influenced by neddylation signaling.

Functional enrichment analyses further supported this observation. CytoSig analysis indicated that CTL and NKT cells were significantly associated with TGFB1-mediated immunosuppressive signaling (Fig. 3M), suggesting functional exhaustion or immune suppression.

KEGG pathway enrichment analysis revealed that distinct metabolic and immune programs across subsets, NK and Treg cells were enriched in proteostasis and metabolic pathways, CD8+ Tem cells were associated with ECM interaction and tissue remodeling pathways, while CTL and NKT cells were enriched in cytotoxicity-related pathways (Fig. 3N). These findings suggest that CD8+ Tem cells represent the major neddylation-active T/NK subset and may play a central role in coordinating immune activation and tumor microenvironment remodeling in LUAD.

3.4 Cellular Interaction and Transcriptional Regulatory Landscape Across LUAD Cell Populations

To investigate how intercellular communication contributes to tumor microenvironment (TME) remodeling in LUAD, we performed comprehensive ligand-receptor interaction analysis across major cell populations. Overall, tumor tissues exhibited markedly increased numbers and strengths of intercellular interactions compared with normal tissues, particularly among epithelial cells, endothelial cells, mast cells, myeloid cells, and T/NK cells (Fig. 4A–C, **Supplementary Fig. 2A–C**), suggesting a globally activated communication network within the tumor microenvironment.

Functional pathway analysis further revealed that multiple oncogenic signaling programs were significantly enriched in tumor tissues, including SPP1, EGF, PARs, EPHA, CD6, ALCAM, periostin (POSTN), OSM, EPHB, PTPRM, and ANGPT signaling pathways (Fig. 4D). In addition, immunomodulatory and extracellular matrix–associated pathways, such as MIF, MHC-I/II, and FN1 signaling, were also markedly elevated, indicating coordinated regulation of immune response, stromal activation, and tissue remodeling in LUAD.

Cell-cell interaction mapping further demonstrated bidirectional communication between immune, stromal, and endothelial compartments. Specifically, T/NK cells were found to interact with endothelial cells through CD99-CD99 and CCL5-ACKR1 axes, and with fibroblasts via CD99-CD99 interactions (Fig. 4E, **Supplementary Fig. 2D,E**). Conversely, endothelial cells and fibroblasts reciprocally regulated T/NK cells through APP-CD74 and COL1A1/2-CD44 signaling, respectively (Fig. 4F). These results suggest the presence of a tightly interconnected signaling network linking immune surveillance with stromal remodeling in LUAD.

To further delineate transcriptional regulatory mechanisms underlying these interactions, DoRothEA analysis identified distinct activation and repression patterns of transcription factors across cell types between tumor and normal tissues. The top 20 transcription factors in T/NK cells are shown in Fig. 4G (**Supplementary Table 4**). Based on these regulators, we constructed a TF-target gene network comprising 41 downstream targets (Fig. 4H, **Supplementary Table 5**), suggesting coordinated transcriptional reprogramming within the T/NK compartment in LUAD.

Importantly, survival analysis revealed that several TF-regulated target genes were significantly associated with patient outcomes. High expression of SFTPC, LITAF, STK17B, EVL, FYN, and LSP1 was associated with favorable prognosis, whereas elevated DNAJB1 expression predicted poor overall survival in LUAD patients (Fig. 4I–O). Receiver operating characteristic (ROC) analysis further demonstrated that all candidate genes exhibited robust prognostic performance, with AUC values exceeding 0.7 (Fig. 4P), supporting their potential clinical relevance. Collectively, these findings suggest that LUAD is characterized by a highly coordinated intercellular communication network coupled with transcriptional reprogramming in T/NK cells, within which DNAJB1 emerges as a key adverse prognostic regulator embedded in the neddylation-associated transcriptional landscape.

3.5 Pseudotime Trajectory Analysis of T/NK Cells in LUAD

To further characterize the developmental dynamics underlying the transcriptional heterogeneity of T/NK cells in LUAD, we performed pseudotime trajectory analysis to infer their differentiation states and lineage progression. The trajectory revealed a major branching event, separating T/NK cells into two distinct developmental fates comprising seven transcriptional states (States 1–7) (Fig. 5A,B), suggesting substantial functional plasticity within this compartment.

Along the inferred trajectory, CD8+ effector memory T cells (CD8+ Tem) in early States 1 and 2 were positioned at the initiation stage, indicating a progenitor-like or less differentiated state within the T/NK continuum. In contrast, cytotoxic T cells (CTL), NK cells, and NKT cells clustered predominantly in States 4 and 5 at the terminal branch, representing more differentiated effector states (Fig. 5C). These results suggest a dynamic transition from early effector-memory-like populations toward terminal cytotoxic differentiation within the LUAD T/NK compartment.

To explore the functional programs underlying these differentiation trajectories, gene set enrichment analysis revealed distinct pathway activations across fate branches. In fate 2, cluster 1 genes were mainly enriched in cytokine–cytokine receptor interaction, IL-17 signaling, and estrogen signaling pathways, suggesting sustained immune ac-

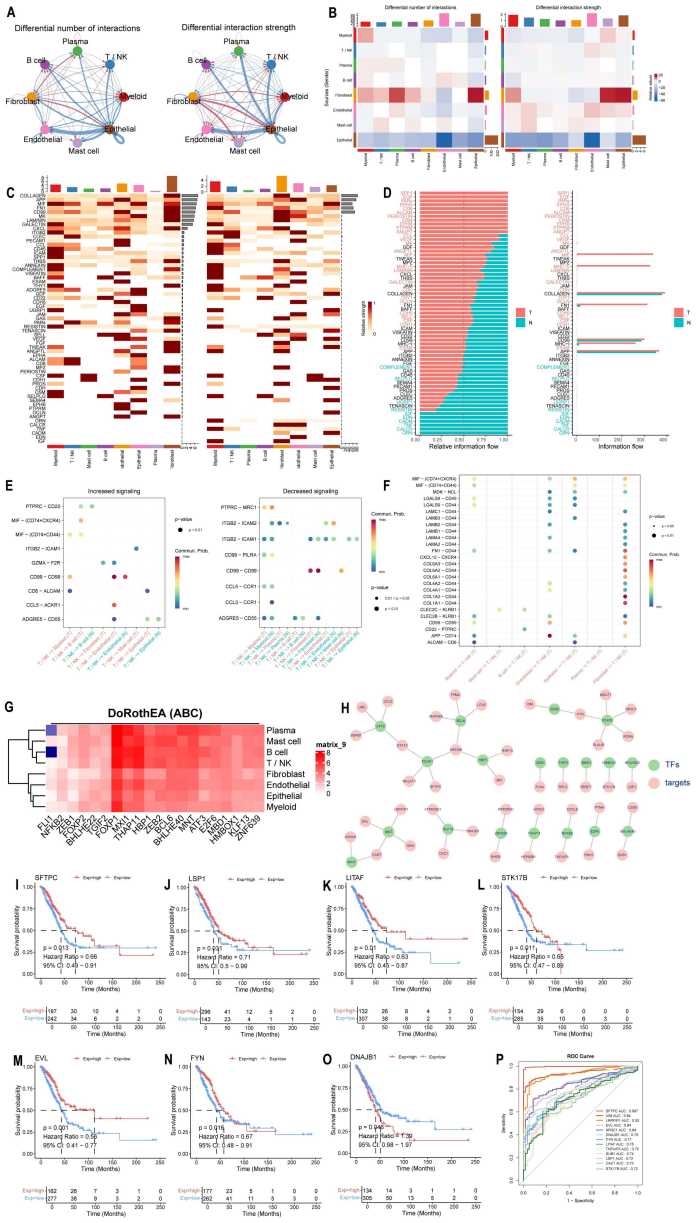

Fig. 4. Cellular interaction and transcriptional regulatory landscape across LUAD cell populations. (A) Cell-cell interaction network among major cell types constructed using CellChat analysis. Node size represents overall interaction weight, and edge thickness indicates interaction strength. (B) Heatmap depicting intercellular communication, including the number of interactions (left panel) and interaction strength (right panel) across cell types. (C) Pattern recognition analysis of incoming and outgoing signaling activities across cell populations. Color intensity represents contribution scores of each cell type. (D) Differential signaling pathway analysis between tumor and normal networks. Pathways enriched in tumor-associated flow are shown in red, those enriched in normal tissues in blue. (E) Bubble plot illustrating increased outgoing signaling from T/NK cells to other cell types in tumor versus normal tissues. (F) Bubble plot illustrating altered incoming signaling to T/NK cells from other cell types in tumor versus normal tissues. (G) Heatmap showing transcription factor (TF) activity profiles across cell types associated with tumor progression in LUAD. (H) TF-target gene regulatory network inferred from transcriptional interaction analysis. (I) Kaplan-Meier survival curves comparing high and low expression of SFTPC in LUAD patients. (J) Kaplan-Meier survival curves comparing high and low expression of LSP1 in LUAD patients. (K) Kaplan-Meier survival curves comparing high and low expression of LITAF in LUAD patients. (L) Kaplan-Meier survival curves comparing high and low expression of STK17B in LUAD patients. (M) Kaplan-Meier survival curves comparing high and low expression of EVL in LUAD patients. (N) Kaplan-Meier survival curves comparing high and low expression of FYN in LUAD patients. (O) Kaplan-Meier survival curves comparing high and low expression of DNAJB1 in LUAD patients. (P) Receiver operating characteristic (ROC) curves evaluating the prognostic performance of SFTPC, VIM, LRRFIP1, EVL, NR3C1, DNAJB1, FYN, LITAF, TNFAIP3, SUB1, LSP1, OAZ1, and STK17B.

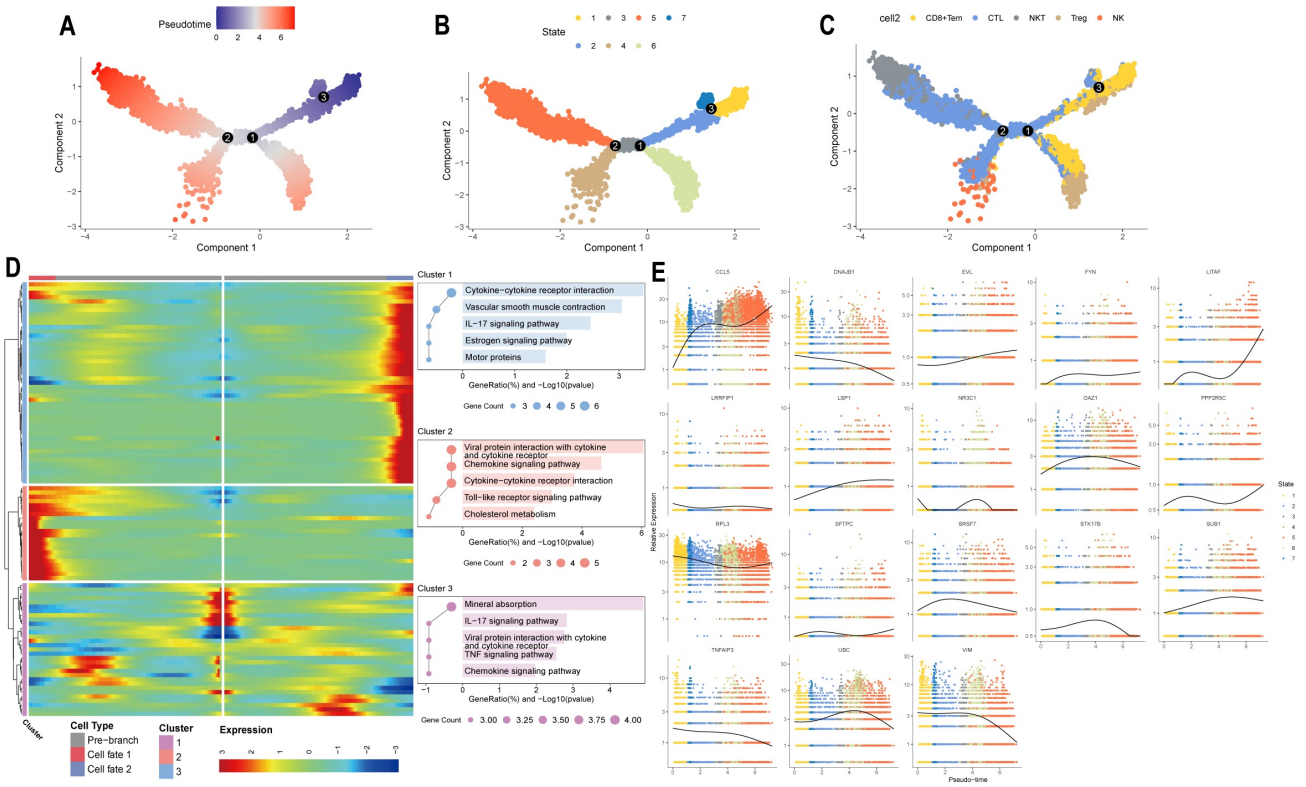

Fig. 5. Pseudotime trajectory of the T/NK subpopulation in LUAD. (A) Pseudotime trajectory of T/NK cells colored by developmental pseudotime, illustrating the dynamic differentiation process. (B) Pseudotime trajectory of T/NK cells colored by cluster identity. (C) Pseudotime trajectory of T/NK cells colored by annotated cell subtypes. (D) Pseudotime heatmap showing dynamically regulated genes during T/NK cell differentiation, grouped into three distinct expression clusters. (E) Pseudotime expression profiles of key genes (CCL5, DNAJB1, EVL, FYN, LITAF, LRRFIP1, LSP1, NR3C1, OAZ1, PPP2R5C, RPL3, SFTPC, SRSF7, STK17B, TNFAIP3, SUB1, UBC, and VIM) across T/NK cell subtypes.

tivation and cytokine responsiveness. Cluster 2 genes, shared across both fate branches, were enriched in viral protein interaction with cytokines and cytokine receptors, chemokine signaling, Toll-like receptor signaling, and cholesterol metabolism, indicating conserved immunometabolic regulation across differentiation states. In addition, cluster 3 genes, specifically activated along fate 2, were significantly enriched in TNF signaling, IL-17 signaling, chemokine signaling, and mineral absorption pathways, reflecting enhanced inflammatory and immune-effector programming in terminal differentiation states (Fig. 5D).

Importantly, transcription factor target gene expression exhibited marked dynamic changes along pseudotime and across differentiation states (Fig. 5E), suggesting that T/NK cell differentiation is accompanied by continuous transcriptional reprogramming. This observation is consistent with the TF regulatory network identified in Fig. 4, supporting a coordinated regulatory architecture underlying both lineage differentiation and functional activation within the T/NK compartment.

Collectively, these findings indicate that T/NK cells in LUAD undergo continuous state transitions from early CD8+ Tem–like populations to terminal cytotoxic phenotypes, accompanied by dynamic rewiring of immune and metabolic pathways, which may be regulated by transcriptional programs associated with neddylation-related signaling.

3.6 Knockdown of the DNAJB1 Inhibits Cell Proliferation, Migration and Invasion in LUAD

Based on multi-omics analyses, DNAJB1 was identified as a candidate oncogene associated with neddylation-related transcriptional programs and poor prognosis in LUAD (Fig. 6A–C), consistent with its potential oncogenic role.

To further investigate its functional significance, DNAJB1 knockdown models were established in A549 and NCI-H1975 LUAD cell lines. Efficient silencing of DNAJB1 was confirmed by qPCR, and sh-DNAJB1 #3 was selected for subsequent functional assays (Fig. 6D). Functional assays revealed that DNAJB1 knockdown significantly reduced cell viability and clonogenic capacity in both LUAD cell lines (Fig. 6E–G), indicating impaired proliferative potential.

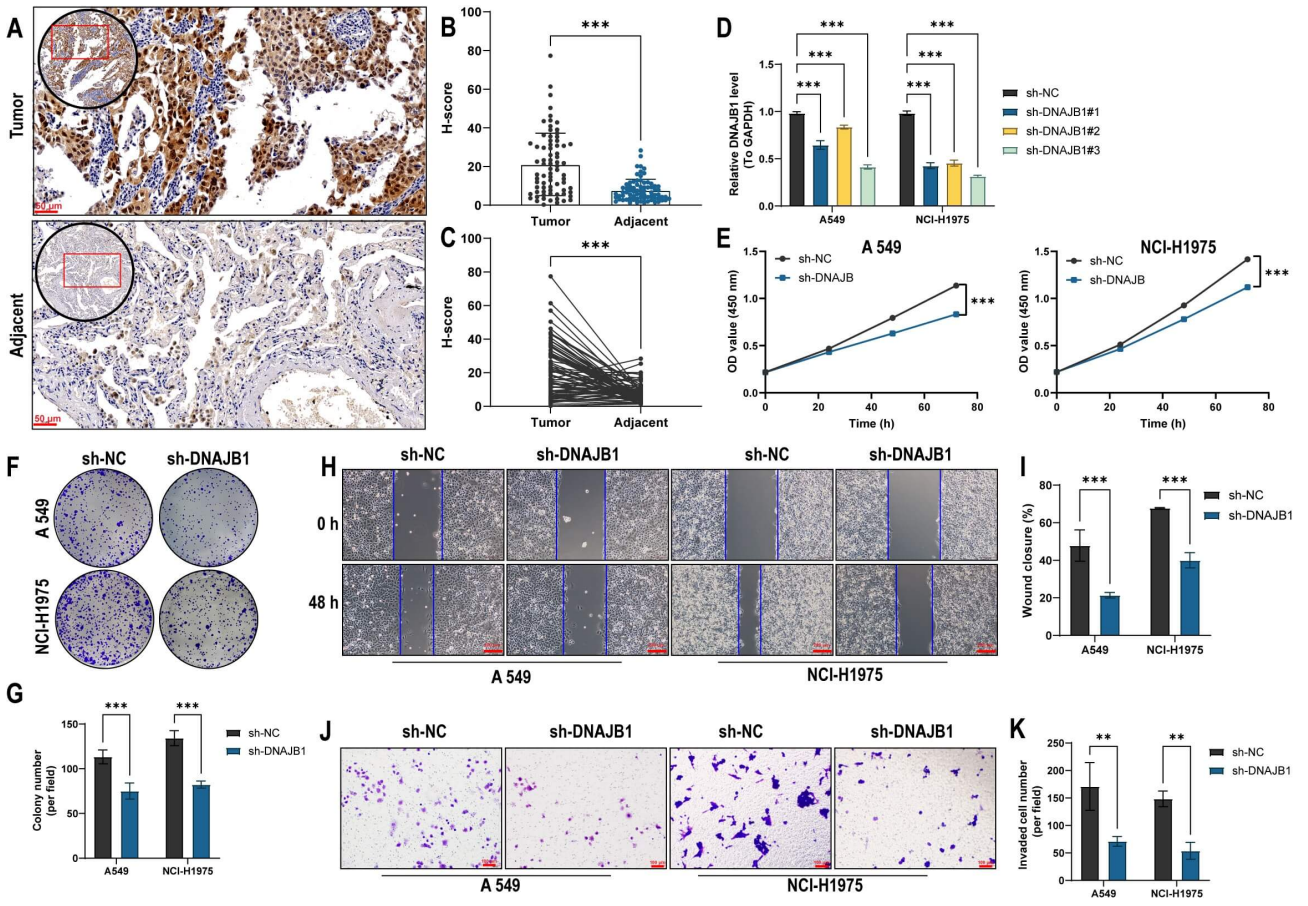

Fig. 6. Knockdown of the DNAJB1 inhibits cell proliferation, migration and invasion in LUAD. (A) Representative immunohistochemical (IHC) images showing DNAJB1 expression in LUAD tissues (n = 75) and adjacent normal tissues (n = 75). Scale bars = 50 μm. (B) Quantification of DNAJB1 IHC staining scores in LUAD tissues. (C) Quantification of DNAJB1 IHC staining scores in adjacent normal tissues. (D) Validation of DNAJB1 knockdown efficiency in A549 and NCI-H1975 cells transfected with sh-DNAJB1-#1, #2, #3 or sh-NC using qPCR. (E) Cell viability of A549 and NCI-H1975 cells measured by CCK-8 assay at 0, 24, 48, and 72 h post-transfection. (F) Representative images of colony formation assays after 2-week culture following transfection. (G) Quantification of colony formation ability in each group. (H) Representative images of wound healing assays at 0 and 48 h post-scratch. Blue dashed lines indicate the initial wound edges and the migrated fronts. Scale bars = 200 μm. (I) Quantification of wound closure rate at 48 h. (J,K) Transwell assays measuring cell invasion, invaded cells counted from three images. Scale bars = 100 μm. Data are presented as mean ± SD. $^{**}p < 0.01$ and $^{***}p < 0.001$.

In addition, wound healing and Transwell assays demonstrated that suppression of DNAJB1 markedly attenuated both migratory and invasive abilities of LUAD cells (Fig. 6H–K). These findings collectively indicate that DNAJB1 contributes to the malignant phenotype of LUAD cells by promoting proliferation, migration, and invasion.

Importantly, these *in vitro* observations are consistent with its identification as a high-risk gene within the neddylation-associated transcriptional landscape, further supporting its potential role as a functionally relevant downstream effector in LUAD progression.

4. Discussion

Increasing evidence suggests that the neddylation pathway participates in tumorigenesis, tumor progression, drug resistance, and tumor recurrence [25,26]. Neddylation is catalyzed by the NEDD8-activating enzyme (NAE) to activate Cullin-RING ligases (CRLs), leading to the deregulation of tumor suppressors and hyperactivation of oncogenic processes in non-small cell lung cancer (NSCLC) [27]. Overexpression of NEDD8 has been shown to enhance migration, invasion, and proliferation of lung cancer cells [28], while also reshaping the tumor immune microenvironment through modulation of myeloid-derived suppressor cell infiltration [29]. Moreover, pharmacological targeting of neddylation has been reported to impair intravascular survival and extravasation of circulating tumor cells, thereby suppressing metastatic dissemination to the lungs [30], highlighting its therapeutic relevance in lung cancer. Although clinical evidence regarding the role of neddy-

lation in treatment response remains limited, sequencing-based analyses and experimental studies have demonstrated that the neddylation pathway may play an important role in responses to anticancer therapies, including immunotherapy and chemotherapy [17,29,31]. Collectively, these studies establish neddylation as a central regulatory axis in LUAD biology.

In the present study, we integrated single-cell and bulk transcriptomic analyses to systematically characterize the neddylation-associated cellular landscape in LUAD. Our results demonstrate that neddylation activity exhibits clear cellular compartment specificity, rather than being uniformly distributed across the tumor microenvironment. Distinct immune, stromal, and epithelial populations display heterogeneous neddylation-associated activity patterns, suggesting multi-level regulation within the tumor microenvironment.

Notably, T/NK cells exhibited the highest neddylation-associated scores among immune compartments, indicating that neddylation may play an important role in regulating immune cell states and functional heterogeneity. Within this population, CD8+ effector memory T cells (CD8+ Tem) represent the most active subset, suggesting their potential sensitivity to neddylation-associated regulatory mechanisms. Cell-cell communication analysis further revealed extensive interactions among immune, stromal, and endothelial compartments, indicating that neddylation-associated signaling is embedded within a highly interconnected tumor microenvironmental network.

CD8+ Tem cells are a key subset of memory CD8+ T cells that play essential roles in antitumor immunity and immune surveillance [32,33]. These cells are characterized by rapid effector responses, enhanced trafficking capacity, and long-term persistence, enabling them to respond swiftly to tumor antigens during disease progression or relapse [33,34]. Functionally, CD8+Tem cells mediate cytotoxicity through granzyme/perforin pathways and inflammatory cytokines such as IFN-γ and TNF-α, thereby contributing to both direct tumor cell killing and immune modulation within the tumor microenvironment [35,36,37]. Importantly, recent studies have demonstrated that neddylation regulates CD8+ T cell metabolic fitness, differentiation, and exhaustion status, thereby influencing antitumor immune responses [38,39]. Inhibition of neddylation can reprogram T cell metabolism toward oxidative phosphorylation and fatty acid oxidation, which are associated with enhanced memory T cell persistence and antitumor activity [38]. These findings provide a mechanistic basis for the observed association between elevated neddylation activity and CD8+ Tem enrichment in our study, and support a dual role of neddylation in both tumor cells and immune compartments.

To reconcile immune-centric findings with tumor-intrinsic functional validation, we adopt a compartment-based model of the tumor microenvironment. Although neddylation activity is predominantly enriched in T/NK cells, transcriptional network analysis identified DNAJB1 as a key prognostic gene associated with LUAD progression. Single-cell analysis further demonstrated that DNAJB1 is broadly expressed across multiple cellular compartments, including malignant epithelial cells, indicating that it is not restricted to immune lineages.

Therefore, DNAJB1 is not interpreted as a T/NK cell-specific effector. Instead, it is proposed as a tumor-intrinsic biomarker embedded within a neddylation-associated tumor microenvironmental context, reflecting coordinated but compartment-specific biological programs. This framework provides a conceptual bridge linking immune-cell neddylation activity with tumor-cell malignant behavior.

DNAJB1 belongs to the HSP40 family and is involved in protein folding, stability, and quality control through interactions with multiple client proteins [40,41]. Notably, DNAJB1 has been implicated in oncogenic processes across multiple cancer types, including its fusion form DNAJB1-PRKACA in fibrolamellar hepatocellular carcinoma [42], as well as its regulatory roles in immune activation and tumor signaling pathways [43,44,45]. In lung cancer, DNAJB1 has been reported to modulate EGFR signaling and therapeutic sensitivity [41]. Consistently, our results demonstrated that DNAJB1 is significantly overexpressed in LUAD and that its knockdown suppresses proliferation, migration, and invasion in LUAD cell lines, supporting its oncogenic role. However, whether DNAJB1 is directly regulated by the neddylation machinery or functions as a downstream effector remains unclear and requires further mechanistic investigation.

In addition to DNAJB1, several TF-associated downstream genes identified in this study, including SFTPC, LITAF, STK17B, EVL, FYN, and LSP1, further refine the functional architecture of the neddylation-associated transcriptional network in LUAD. Rather than representing isolated gene-level associations, these genes collectively define distinct biological modules involving immune regulation, epithelial homeostasis, cytoskeletal remodeling, and inflammatory signaling.

Specifically, FYN [46,47], STK17B [48], and LSP1 [49,50] are key regulators of T cell receptor signaling, immune activation thresholds, and leukocyte trafficking, suggesting that neddylation-associated transcriptional activity may influence both T cell activation and immune cell infiltration. EVL contributes to actin cytoskeleton dynamics and immune cell motility, potentially affecting cellular migration within the tumor microenvironment [51]. SFTPC reflects epithelial cell-specific homeostatic regulation in lung tissue [52], while LITAF is involved in TNF-α-mediated inflammatory signaling pathways.

Collectively, these genes indicate that the neddylation-associated transcriptional network in LUAD is functionally heterogeneous and operates across multiple biological compartments. This multi-module organization further supports

the concept that neddylation influences both immune and tumor epithelial programs in a coordinated manner within the tumor microenvironment.

Limitation

Despite the comprehensive multi-omics integration approach adopted in this study, several limitations should be acknowledged. First, the construction of neddylation-related cellular landscapes and biomarker identification relied primarily on publicly available transcriptomic datasets. Although these datasets provide high-resolution insights into LUAD biology, inherent limitations such as batch effects, inter-individual heterogeneity, and differences in sample processing may introduce potential biases and affect the robustness of the findings.

Second, the single-cell RNA sequencing dataset used in this study was derived from a Korean LUAD cohort. Therefore, the observed cellular composition, transcriptional programs, and neddylation-associated activity may partly reflect population-specific or region-specific biological characteristics. The generalizability of these findings to other ethnic groups or broader LUAD populations remains to be further validated using independent multi-ethnic single-cell cohorts.

Third, although we experimentally validated the expression and functional role of DNAJB1 *in vitro*, additional *in vivo* validation was not performed due to experimental constraints. Future animal studies are necessary to further validate its biological and therapeutic relevance.

Finally, while our analysis identified a strong association between DNAJB1 and neddylation-related transcriptional programs, direct biochemical evidence linking DNAJB1 to the neddylation machinery remains lacking. Therefore, DNAJB1 should be interpreted as a neddylation-associated biomarker rather than a neddylation-regulated gene. Future studies incorporating NEDD8 pathway inhibition (e.g., MLN4924), protein interaction assays, and proteomic profiling will be necessary to determine whether DNAJB1 is directly regulated by or functionally integrated into the neddylation system.

5. Conclusion

In conclusion, we integrated single-cell and bulk RNA-sequencing data to characterize the neddylation-related cellular landscape, cell-cell interactions, pseudotime trajectories, and biomarkers in LUAD. We also validated biomarker expression and function using clinical specimens and *in vitro* assays. Our findings provide new insights into the post-translational modification mechanisms underlying LUAD progression and identify DNAJB1 as a promising therapeutic target for LUAD treatment.

Availability of Data and Materials

Publicly available datasets were analyzed in this study. The scRNA-seq data were obtained from the Gene Expression Omnibus (GEO; GSE131907), and bulk RNA-seq data were obtained from the Cancer Genome Atlas (TCGA, https://www.cancer.gov/about-nci/organization/ccg/research/structural-genomics/tcga). Additional processed data were accessed from the UCSC Xena website (https://xenabrowser.net/datapages/), and neddylation-related gene sets were retrieved from the Molecular Signatures Database (MSigDB, https://www.gsea-msigdb.org/gsea/msigdb/). The canonical marker genes were obtained from the CellMarker database (http://117.50.127.228/CellMarker/). All datasets used in this study are openly accessible through the respective repositories. The datasets used and analyzed during the current study are available from the corresponding author upon reasonable request.

Author Contributions

XP and GS designed the study. GX conducted the bioinformatic analysis and analyzed the data. GX performed the experiments and analyzed the data. XP drafted the manuscript. XP and GS reviewed and revised the manuscript. All authors contributed to the article and approved the submitted version. All authors contributed to editorial changes in the manuscript. All authors read and approved the final manuscript. All authors have participated sufficiently in the work and agreed to be accountable for all aspects of the work.

Ethics Approval and Consent to Participate

Not applicable.

Acknowledgment

We gratefully acknowledge the GEO, TCGA, and UCSC Xena databases and the uploader of the datasets.

Funding

This research received no external funding.

Conflicts of Interest

The authors declare no conflicts of interest.

Supplementary Material

Supplementary material associated with this article can be found, in the online version, at https://doi.org/10.31083/FBL52485.

References

[1] Bray F, Laversanne M, Sung H, Ferlay J, Siegel RL, Soerjomataram I, et al. Global cancer statistics 2022: GLOBOCAN estimates of incidence and mortality worldwide for 36 cancers in 185 countries. CA: a Cancer Journal for Clinicians. 2024; 74: 229–263. https://doi.org/10.3322/caac.21834

[2] Luo G, Zhang Y, Rumgay H, Morgan E, Langselius O, Vignat J, et al. Estimated worldwide variation and trends in incidence of lung cancer by histological subtype in 2022 and over time: a population-based study. The Lancet. Respiratory Medicine.

2025; 13: 348–363. https://doi.org/10.1016/S2213-2600(24)00428-4

[3] Allemani C, Matsuda T, Di Carlo V, Harewood R, Matz M, Nikšić M, et al. Global surveillance of trends in cancer survival 2000-14 (CONCORD-3): analysis of individual records for 37 513 025 patients diagnosed with one of 18 cancers from 322 population-based registries in 71 countries. Lancet (London, England). 2018; 391: 1023–1075. https://doi.org/10.1016/S0140-6736(17)33326-3

[4] Murphy C, Pandya T, Swanton C, Solomon BJ. Lung Cancer in Nonsmoking Individuals: A Review. JAMA. 2025; 334: 1836–1845. https://doi.org/10.1001/jama.2025.17695

[5] Heymach JV, Harpole D, Mitsudomi T, Taube JM, Galffy G, Hochmair M, et al. Perioperative Durvalumab for Resectable Non-Small-Cell Lung Cancer. The New England Journal of Medicine. 2023; 389: 1672–1684. https://doi.org/10.1056/NEJMoa2304875

[6] Spicer JD, Garassino MC, Wakelee H, Liberman M, Kato T, Tsuboi M, et al. Neoadjuvant pembrolizumab plus chemotherapy followed by adjuvant pembrolizumab compared with neoadjuvant chemotherapy alone in patients with early-stage non-small-cell lung cancer (KEYNOTE-671): a randomised, double-blind, placebo-controlled, phase 3 trial. Lancet (London, England). 2024; 404: 1240–1252. https://doi.org/10.1016/S0140-6736(24)01756-2

[7] Balbi M, Capelli S, Caroli A, Culasso NC, Barba M, Senkeev R, et al. CT-Guided Core Needle Biopsy of Pulmonary Lesions Associated With Cystic Airspaces: A Case-Control Study. AJR. American Journal of Roentgenology. 2024; 223: e2431042. https://doi.org/10.2214/AJR.24.31042

[8] Baratella E, Cernic S, Minelli P, Furlan G, Crimì F, Rocco S, et al. Accuracy of CT-Guided Core-Needle Biopsy in Diagnosis of Thoracic Lesions Suspicious for Primitive Malignancy of the Lung: A Five-Year Retrospective Analysis. Tomography (Ann Arbor, Mich.). 2022; 8: 2828–2838. https://doi.org/10.3390/tomography8060236

[9] Fang C, Liu C, Qi R, Ding J, Luo T, Yu F, et al. Integrated Analysis of Single-cell and Bulk-RNA Sequencing Data to Identify Redox-related Genes as Prognostic Biomarkers and Therapeutic Targets of Lung Adenocarcinoma With Osimertinib Resistance. Frontiers in Bioscience (Landmark Edition). 2025; 30: 40454. https://doi.org/10.31083/fbl40454

[10] Chen F, Ma J, Hu S, Wu C, Chen S, Lin J. Prognostic Cell Death Index for Lung Adenocarcinoma: A Comprehensive Transcriptome-Based Analysis of Twelve Programmed Cell Death Pattern Genes. Frontiers in Bioscience (Landmark Edition). 2024; 29: 135. https://doi.org/10.31083/j.fbl2904135

[11] Zhang S, Yu Q, Li Z, Zhao Y, Sun Y. Protein neddylation and its role in health and diseases. Signal Transduction and Targeted Therapy. 2024; 9: 85. https://doi.org/10.1038/s41392-024-01800-9

[12] Enchev RI, Schulman BA, Peter M. Protein neddylation: beyond cullin-RING ligases. Nature Reviews. Molecular Cell Biology. 2015; 16: 30–44. https://doi.org/10.1038/nrm3919

[13] Kamitani T, Kito K, Nguyen HP, Yeh ET. Characterization of NEDD8, a developmentally down-regulated ubiquitin-like protein. The Journal of Biological Chemistry. 1997; 272: 28557–28562. https://doi.org/10.1074/jbc.272.45.28557

[14] Jones J, Wu K, Yang Y, Guerrero C, Nillegoda N, Pan ZQ, et al. A targeted proteomic analysis of the ubiquitin-like modifier nedd8 and associated proteins. Journal of Proteome Research. 2008; 7: 1274–1287. https://doi.org/10.1021/pr700749v

[15] Zhou L, Jiang Y, Luo Q, Li L, Jia L. Neddylation: a novel modulator of the tumor microenvironment. Molecular Cancer. 2019; 18: 77. https://doi.org/10.1186/s12943-019-0979-1

[16] Xie P, Peng Z, Chen Y, Li H, Du M, Tan Y, et al. Neddylation of PTEN regulates its nuclear import and promotes tumor development. Cell Research. 2021; 31: 291–311. https://doi.org/10.1038/s41422-020-00443-z

[17] Mao H, Lin X, Sun Y. Neddylation Regulation of Immune Responses. Research (Washington, D.C.). 2023; 6: 0283. https://doi.org/10.34133/research.0283

[18] Zhou L, Zhang W, Sun Y, Jia L. Protein neddylation and its alterations in human cancers for targeted therapy. Cellular Signalling. 2018; 44: 92–102. https://doi.org/10.1016/j.cellsig.2018.01.009

[19] Zhou L, Jia L. Targeting Protein Neddylation for Cancer Therapy. Advances in Experimental Medicine and Biology. 2020; 1217: 297–315. https://doi.org/10.1007/978-981-15-1025-0_18

[20] He ZX, Yang WG, Zengyangzong D, Gao G, Zhang Q, Liu HM, et al. Targeting cullin neddylation for cancer and fibrotic diseases. Theranostics. 2023; 13: 5017–5056. https://doi.org/10.7150/thno.78876

[21] Jiang P, Zhang Y, Ru B, Yang Y, Vu T, Paul R, et al. Systematic investigation of cytokine signaling activity at the tissue and single-cell levels. Nature Methods. 2021; 18: 1181–1191. https://doi.org/10.1038/s41592-021-01274-5

[22] Decker JT, Hall MS, Nanua D, Orbach SM, Roy J, Angadi A, et al. Dynamic Transcriptional Programs During Single NK Cell Killing: Connecting Form to Function in Cellular Immunotherapy. Cellular and Molecular Bioengineering. 2024; 17: 177–188. https://doi.org/10.1007/s12195-024-00812-3

[23] Zhang Z, Li Y, Wang M, Jing Y, Hu H, Shi M, et al. Identification of differentiation markers and immune microenvironment in head and neck squamous cell carcinoma using machine learning combined with single-cell analysis. Translational Cancer Research. 2025; 14: 8579–8599. https://doi.org/10.21037/tcr-2025-1723

[24] Qiu X, Hill A, Packer J, Lin D, Ma YA, Trapnell C. Single-cell mRNA quantification and differential analysis with Census. Nature Methods. 2017; 14: 309–315. https://doi.org/10.1038/nmeth.4150

[25] Naik SK, Lam EWF, Parija M, Prakash S, Jiramongkol Y, Adhya AK, et al. NEDDylation negatively regulates ERRβ expression to promote breast cancer tumorigenesis and progression. Cell Death & Disease. 2020; 11: 703. https://doi.org/10.1038/s41419-020-02838-7

[26] Powell RT, Rinkenbaugh AL, Guo L, Cai S, Shao J, Zhou X, et al. Targeting neddylation and sumoylation in chemoresistant triple negative breast cancer. NPJ Breast Cancer. 2024; 10: 37. https://doi.org/10.1038/s41523-024-00644-4

[27] Qin A, Wells L, Malhotra B, Gadgeel S, Schneider BJ, Ramnath N, et al. A Phase II Trial of Pevonedistat and Docetaxel in Patients With Previously Treated Advanced Non-Small-Cell Lung Cancer. Clinical Lung Cancer. 2024; 25: 128–134. https://doi.org/10.1016/j.cllc.2023.10.011

[28] Liu H, Shih YH, Wang WL, Chang WL, Wang YC. UBE1C is upregulated and promotes neddylation of p53 in lung cancer. FASEB Journal: Official Publication of the Federation of American Societies for Experimental Biology. 2023; 37: e23181. https://doi.org/10.1096/fj.202300629R

[29] Zhou L, Lin X, Zhang L, Chen S, Chen J, Zhou Z, et al. Neddylation pathway promotes myeloid-derived suppressor cell infiltration via NF-κB-mCXCL5 signaling in lung cancer. International Immunopharmacology. 2022; 113: 109329. https://doi.org/10.1016/j.intimp.2022.109329

[30] Jiang Y, Liang Y, Li L, Zhou L, Cheng W, Yang X, et al. Targeting neddylation inhibits intravascular survival and extravasation of cancer cells to prevent lung-cancer metastasis. Cell Biology and Toxicology. 2019; 35: 233–245. https://doi.org/10.1007/s10565-019-09472-w

[31] Cui Y, Chen Z, Pan B, Chen T, Ding H, Li Q, et al. Neddylation pattern indicates tumor microenvironment characterization and predicts prognosis in lung adenocarcinoma. Frontiers in Cell and Developmental Biology. 2022; 10: 979262. https://doi.org/10.3389/fcell.2022.979262

[32] Turner SJ, Bennett TJ, La Gruta NL. $CD8^+$ T-Cell Memory: The Why, the When, and the How. Cold Spring Harbor Perspectives in Biology. 2021; 13: a038661. https://doi.org/10.1101/cshperspect.a038661

[33] Han J, Khatwani N, Searles TG, Turk MJ, Angeles CV. Memory $CD8^+$ T cell responses to cancer. Seminars in Immunology. 2020; 49: 101435. https://doi.org/10.1016/j.smim.2020.101435

[34] Reading JL, Gálvez-Cancino F, Swanton C, Lladser A, Peggs KS, Quezada SA. The function and dysfunction of memory $CD8^+$ T cells in tumor immunity. Immunological Reviews. 2018; 283: 194–212. https://doi.org/10.1111/imr.12657

[35] Chuensirikulchai K, Pata S, Laopajon W, Takheaw N, Kotemul K, Jindaphun K, et al. Identification of different functions of $CD8^+$ T cell subpopulations by a novel monoclonal antibody. Immunology. 2024; 173: 321–338. https://doi.org/10.1111/imm.13826

[36] Reiser J, Banerjee A. Effector, Memory, and Dysfunctional CD8(+) T Cell Fates in the Antitumor Immune Response. Journal of Immunology Research. 2016; 2016: 8941260. https://doi.org/10.1155/2016/8941260

[37] Li J, Wu C, Hu H, Qin G, Wu X, Bai F, et al. Remodeling of the immune and stromal cell compartment by PD-1 blockade in mismatch repair-deficient colorectal cancer. Cancer Cell. 2023; 41: 1152–1169.e7. https://doi.org/10.1016/j.ccell.2023.04.011

[38] Jiménez-Lasheras B, Velasco-Beltrán P, Egia-Mendikute L, Pérez-Gutiérrez L, Lee SY, de Blas A, et al. NEDDylation Regulates CD8+ T-cell Metabolism and Antitumor Immunity. Cancer Immunology Research. 2025; 13: 1004–1021. https://doi.org/10.1158/2326-6066.CIR-24-0127

[39] Ren H, Luan Z, Zhang R, Zhang H, Bian C. A novel approach to explore metabolic diseases: Neddylation. Pharmacological Research. 2024; 210: 107532. https://doi.org/10.1016/j.phrs.2024.107532

[40] Mitra A, Shevde LA, Samant RS. Multi-faceted role of HSP40 in cancer. Clinical & Experimental Metastasis. 2009; 26: 559–567. https://doi.org/10.1007/s10585-009-9255-x

[41] Park SY, Choi HK, Seo JS, Yoo JY, Jeong JW, Choi Y, et al. DNAJB1 negatively regulates MIG6 to promote epidermal growth factor receptor signaling. Biochimica et Biophysica Acta. 2015; 1853: 2722–2730. https://doi.org/10.1016/j.bbamcr.2015.07.024

[42] Shirani M, Levin S, Shebl B, Requena D, Finkelstein TM, Johnson DS, et al. Increased Protein Kinase A Activity Induces Fibrolamellar Hepatocellular Carcinoma Features Independent of DNAJB1. Cancer Research. 2024; 84: 2626–2644. https://doi.org/10.1158/0008-5472.CAN-23-4110

[43] Bauer J, Köhler N, Maringer Y, Bucher P, Bilich T, Zwick M, et al. The oncogenic fusion protein DNAJB1-PRKACA can be specifically targeted by peptide-based immunotherapy in fibrolamellar hepatocellular carcinoma. Nature Communications. 2022; 13: 6401. https://doi.org/10.1038/s41467-022-33746-3

[44] Zhao B, Yang J, Ran F, Shi Y, Yang L, Duan Y, et al. CircBIRC6 affects prostate cancer progression by regulating miR-574-5p and DNAJB1. Cancer Biology & Therapy. 2024; 25: 2399363. https://doi.org/10.1080/15384047.2024.2399363

[45] Yin Y, Zhang J, Ma T, Chen D, Lu D. miR-1205/DNAJB1 reverses docetaxel chemoresistance in human triple negative breast carcinoma cells via regulation of mutp53/TAp63 signaling. Acta Biochimica et Biophysica Sinica. 2022; 54: 37–46. https://doi.org/10.3724/abbs.2021006

[46] Elias D, Ditzel HJ. Fyn is an important molecule in cancer pathogenesis and drug resistance. Pharmacological Research. 2015; 100: 250–254. https://doi.org/10.1016/j.phrs.2015.08.010

[47] Peng S, Fu Y. FYN: emerging biological roles and potential therapeutic targets in cancer. Journal of Translational Medicine. 2023; 21: 84. https://doi.org/10.1186/s12967-023-03930-0

[48] Scheuplein F, Renner F, Campbell JE, Campbell R, De Savi C, Eckmann J, et al. Evaluation of STK17B as a cancer immunotherapy target utilizing highly potent and selective small molecule inhibitors. Frontiers in Immunology. 2024; 15: 1411395. https://doi.org/10.3389/fimmu.2024.1411395

[49] Zhu P, Gu J, Luo Y, Xi Y. Leukocyte-specific protein 1 (LSP1): A key regulator of cytoskeletal dynamics and leukocyte function. Xi Bao Yu Fen Zi Mian Yi Xue Za Zhi = Chinese Journal of Cellular and Molecular Immunology. 2025; 41: 750–755. (In Chinese)

[50] Xu D, Zhou X, Min S, Zhang Y, Zhu X, Qiao K, et al. Leukocyte-specific protein 1 is associated with the stage and tumor immune infiltration of cervical cancer. Scientific Reports. 2025; 15: 7566. https://doi.org/10.1038/s41598-025-91066-0

[51] Waldman MM, Rahkola JT, Sigler AL, Chung JW, Willett BAS, Kedl RM, et al. Ena/VASP Protein-Mediated Actin Polymerization Contributes to Naïve $CD8^+$ T Cell Activation and Expansion by Promoting T Cell-APC Interactions *In Vivo*. Frontiers in Immunology. 2022; 13: 856977. https://doi.org/10.3389/fimmu.2022.856977

[52] Nureki SI, Tomer Y, Venosa A, Katzen J, Russo SJ, Jamil S, et al. Expression of mutant Sftpc in murine alveolar epithelia drives spontaneous lung fibrosis. The Journal of Clinical Investigation. 2018; 128: 4008–4024. https://doi.org/10.1172/JCI99287